Title

Soft X-ray spectroscopy studies of adsorption and reaction of CO in the presence of H2 over 6nm MnO nanoparticles supported on mesoporous Co3O4

Authors

Ralston, Walter T
Musselwhite, Nathan
Kennedy, Griffin
et al.

Publication Date

2016-06-01

DOI

10.1016/j.susc.2015.12.006

Peer reviewed

Soft X-ray Spectroscopy Studies of Adsorption and Reaction of CO in the presence of H_2 over 6 nm MnO Nanoparticles Supported on Mesoporous Co_3O_4

[†‡]Walter T. Ralston, [†‡]Nathan Musselwhite, [†‡]Griffin Kennedy, [†‡]Kwangjin An, [†‡]Yonatan Horowitz, [‡]Amy Cordones-Hahn, [‡‖]Bruce Rude, [‡]Musahid Ahmed, [*†‡]Gerome Melaet and [*‡]Selim Alayoglu

[‡]Chemical Sciences Division & Advanced Light Source, Lawrence Berkeley National Laboratory,
[†]Department of Chemistry, UC Berkeley

Abstract

Keywords: ambient pressure X-ray photoelectron spectroscopy, in situ x-ray absorption spectroscopy, manganese oxide nanoparticles, mesoporous spinel cobalt oxide, CO hydrogenation

Abbreviations: ambient pressure X-ray photoelectron spectroscopy (APXPS), X-ray absorption spectroscopy (XAS), total electron yield (TEY), transmission electron microscopy (TEM), high resolution transmission electron microscopy (HRTEM), scanning transmission electron microscopy (STEM), energy dispersive spectroscopy (EDS), electron energy loss spectroscopy (EELS), scanning transmission X-ray microscopy (STXM), nanoparticles (NPs).

1. Introduction

Introduction is still a work in progress! ☺

In honor of Professor Gabor A. Somorjai's 80th birthday this year…we would like to demonstrate the strategies taken to characterize heterogeneous catalyst surfaces in an effort to understand catalytic trends and surface transformations whilst informing future catalyst designs.

In order to bridge the so-called 'materials gap' in surface science the Somorjai group has utilized colloidal synthesis strategies to produce well-defined nanoparticles that serve as model catalysts. There have been many case examples of size [1–10,3,11], shape [12–20] and composition [12,21–23] controlled nanoparticles for a variety of applications, providing a wide array of model systems.

The study of these materials' surfaces has become possible with the proliferation of high intensity X-ray sources (ref) and specialized instrumentation (ref) allowing for *in-situ* spectroscopic characterization at pressures above high vacuum. The dynamic nature of surfaces has been well-documented (ref), highlighting the importance of studying a catalyst's surface under reaction conditions.

Example of nanoparticle studies; lead into this study

Recently, 6nm MnO_x nanoparticles supported on mesoporous Co_3O_4 was reported to produce high yields of methanol from a H_2/CO_2 (3:1) feed, where the enhanced catalytic activity towards methanol was attributed to the unique oxide-oxide interface (ref). Bimetallic Co-Mn nanoparticles supported on carbon nanofibers [35], titania [36], and silica [37] have been studied under CO hydrogenation conditions (Fischer-Tropsch synthesis) and are reported to promote long chain hydrocarbons over methane. These studies over Co-Mn systems have captured unique catalytic behaviors and trends for well-defined, model hybrid systems; yet the molecular origins of the observed surface phenomena remain less understood. In this study, we investigated the surface chemical structure of 6nm MnO nanoparticles supported on a mesoporous Co_3O_4 co-catalyst under CO hydrogenation conditions using ambient pressure X-ray photoelectron spectroscopy (APXPS) and *in-situ* X-ray absorption spectroscopy (XAS) in the total electron yield (TEY) mode. Measurements were made under oxidizing (O_2), reducing (H_2) and reactive (H_2 + CO; 2:1) conditions. In addition, *ex-situ* electron and X-ray spectro-microscopy techniques were employed to determine morphology, chemical compositions and elemental distributions for the pre- and post-reaction catalysts.

2. Experimental

2.1. Synthesis of MnO Nanoparticles / Mesoporous Co_3O_4 Catalyst

The synthesis of 6 nm MnO NPs [38] and mesoporous Co_3O_4 support [39] has been described in detail elsewhere. Briefly, MnO NPs were synthesized by refluxing 1.24 g manganese oleate (~2 mmol) dissolved in 10 g of 1-octadecene for 10 min. MnO NPs were stored in 10 ml of chloroform until further use.

Mesoporous Co_3O_4, (m-Co_3O_4) was prepared using a hard template (39). A mixture of cobalt (II) nitrate hexahydrate (4.7 g) in 8 ml of water and KIT-6 (4.0 g) dissolved in 50 ml of toluene were evaporated at 65 °C and the precipitated solid was subsequently calcined at 300 °C for 6 h in air. The KIT-6 template was dissolved using an aqueous solution of 2 M NaOH at 60 °C.

The MnO NPs / m-Co_3O_4 catalyst was prepared via the capillary inclusion method(**ref**). To produce a catalyst of nominally 10 weight % Mn, 2 mL of the colloidal MnO_x NPs were diluted with 40 mL of *n*-hexane and mixed with 250 mg of m-Co_3O_4. The mixture was sonicated for 3 h at room temperature. The precipitate was collected by centrifugation and washed with a 50:50 v/v mixture of acetone and ethanol. The precipitated solid was dried at 80 °C overnight.

2.2. Soft X-ray Absorption Spectroscopy

Soft X-ray absorption spectroscopy (XAS) studies were performed in beamline 6.0.2 of the Advanced Light Source (ALS). A purpose-built XAS end-station (Spectroscopy and Reactivity Probe for Catalyst Research) was employed for the measurements. The end-station consists of three vacuum chambers: an entrance chamber, an ambient pressure (AP) cell, and a mass spectrometry chamber.

The entrance chamber consists of a variable aperture exit slit and an aluminum mesh for I_0 correction. A base pressure of 10^{-8} Torr is maintained in the entrance chamber at any time. An exit slit of 50 µm diameter was used for the measurements reported in this paper. The entrance chamber is separated from the AP cell with a 100 nm thick Si_3N_4 window (1 mm by 0.5 mm, Silson Inc.).

The AP cell can be dosed using leak valves or a dedicated pre-mixing line with reactive/inert gases in the 0.01-1000 Torr range. Gas pressure in the AP cell and pre-mixing line were monitored via capacitance (Baratron, MKS) and cold cathode (Pfeifer and Granville-Phillips) gauges located at various points. To ensure a continuously well-mixed gas environment, a motorized fan is placed in close proximity to the sample holder.

Sample holder is installed on a 2.75” CF flange with four mini flange ports, and is mobilized on a top-mounted XYZΩ stage. Samples of nanoparticle films on 200 µm Si wafers or ~200 µm pelletized powders are secured between a 1/16” metal plate, which is used for total electron yield current measurements, and a 1/16” cylindrical ceramic spacer (Al_2O_3). A 1/32” metal foil with a central hole (φ~1/4”) is attached to the front end of the ceramic spacer, and used to apply

bias to sample. The metal current plate sits on a PID-powered ceramic heater (φ~1" and 10-16 ohm resistance, Momentive), which allows sample temperatures in the 25-550°C range. A photodiode (SXUV100, Opto Diode Corp.) is placed on a Z-manipulator and adjusted towards or away from sample for fluorescence measurements.

The mass spectrometer chamber is separated from the AP cell with a gate valve. A quadruple mass spectrometer (Stanford Research Systems) is used for continuous, on-line detection. To achieve this, 1/8" stainless steel tubing, heated to 100°C, is run between the sample front and the mass spectrometer ionizer. The sample end of the carrier tubing is manually adjusted to optimize detection sensitivity.

In a typical XAS experiment, Co L_3, Mn L_3, O K, and C K absorption edge spectra were monitored in total electron yield (TEY) mode in oxidizing, reducing, or reaction conditions. The current to sample was measured using an amplifier with a bias potential of 250 V. Before measurements samples were treated for 0.5 hours in oxidizing or reducing conditions, or for 1 to 12 hours under reaction atmospheres. All spectra were normalized for I_0.

2.3. Ambient Pressure X-ray Photoelectron Spectroscopy

The APXPS chamber in beamline 9.3.2 at the ALS has been described elsewhere [40]. Various photon energies were used to probe the 2p and 3p levels of Co and Mn, in addition to the 1s levels of C and O.

number the conditions below for reference later on?

The order of the APXPS experimental conditions was as follows: oxidation of the catalyst in 200 mTorr O_2 at 350°C, reduction of the catalyst in 200 mTorr H_2 at 250°C, reaction conditions of 300 mTorr H_2+CO (2:1) at 225°C, followed by higher reduction temperatures of 350 and 480°C under 200 mTorr H_2 each followed by reaction conditions at 225°C.

After the previous experimental conditions, the reversibility of the surface changes was studied whereby the catalyst was re-oxidized in O_2 at 350°C, reduced in H_2 at 250°C, and run under reaction conditions at 225°C. Energy calibrations were performed using valence level XPS spectra at each photon energy. XPS peaks for gas phase O_2 and CO were also used for energy calibration. XPS data and error analysis was carried out using CasaXPS software.

For a given pressure and temperature condition, X-ray spectra were measured, usually for an hour or more, until no further change in the spectra was observed. The acquisition time of each X-ray technique is however varied: 7 min for NEXAFS TEY and 40 min for STXM. Likewise, typical exposure times for the APXPS experiments were in the order of hours during which multiple measurements, at various core (Co and Mn 2p; C and O 1s) and valence levels using different photon energies (900 eV for Co 2p, 760 eV for Mn 2p, 630 eV for C and O), were made until no further change in the spectral features could be detected. Note, that all the techniques showed the evidence of reduction (or oxidation) of Co and Mn for the MnO/Co_3O_4 catalyst, starting with the first measurement, and no significant change in the course of any experiment

at any given condition. This suggests that the steady-state was reached rather quickly in the timescale of any X-ray technique used. – this section will be rewritten

2.4. Scanning Transmission X-ray Microscopy (STXM)

STXM experiments were performed at the molecular environmental sciences beamline (11.0.2) at the ALS [41]. Samples were dropcasted from suspensions in methanol on to 100 nm thick Si_3N_4 windows, and air-dried before measurements. Multiple particles each measuring approximately 500 nm, were measured at both Mn L and Co L absorption edges with spatial resolutions better than 40 nm. Image stacking, alignment, and spectral integrations were carried out using AXIS software.

2.5. Scanning Transmission Electron Microscopy (STEM) with Energy Dispersive Spectroscopy (EDS) and Electron Energy Loss Spectroscopy (EELS)

TEM and STEM measurements were performed at an accelerating voltage of 200 kV using a Jeol2100F transmission electron microscope equipped with an INCA energy dispersive spectrometer and a Gatan Tridiem electron energy loss spectrometer. TEM samples were prepared by dropcasting catalyst suspensions in methanol on to lacey carbon supported on Cu grids and vacuum-dried at 100°C for 2 days before measurements. EDS was carried out by monitoring Co and Mn K lines. EELS was carried out using convergence and collection semi-angles of 12mrad with ~1 eV energy resolution at a dispersion of 0.2 eV per channel. Standard Gatan software was utilized for the analysis of EELS spectra; the pre-edge background was subtracted using a power-law fit while Hartree-Slater cross-sections were used to subtract step edges before quantification.

3. Results and Discussion

3.1. Characterization of the As-Prepared Catalyst

The 6 nm MnO NPs / m-Co_3O_4 catalyst was characterized prior to in situ studies using a combination of techniques. TEM and STEM images show ordered mesopores of about 10 nm in size (Figures S1a and S1c). TEM and HRTEM images display nanocrystalline grains with sizes in the 5-10 nm range (Figures S1a and S1b). Individual MnO NPs could not be discerned from the TEM images. Mesoporous particles were measured to be in the range of 0.2-2 µm, based on TEM images. STEM/EDS elemental maps indicated random and uniform distributions of Mn over the Co matrix (Figures S1c-S1e). STEM/EDS maps and averages of multiple STEM/EELS point spectra show Mn:Co ratios of 0.1, which is consistent with the nominal mixing of MnO NPs and mesoporous Co_3O_4.

regular TEM image of particles (for SI at least?)

STXM images taken pre- and post- metal edges (Mn L and Co L) indicated random and uniform distribution of Co and Mn components across single particles, and thus was consistent with STEM/EDS maps. STXM also indicated particle cores and shells were chemically uniform;

spinel Co_3O_4 and mixtures of Mn^{2+} and Mn^{3+} species, obtained from a qualitative inspection of STXM spectra (Figure S2).

3.2. Ambient Pressure X-ray Photoelectron Spectroscopy

3.2.1 Co and Mn spectra

Figure 1a shows Mn and Co 3p core levels monitored using 630 eV photons, and demonstrates invariably larger fractions of MnO_x ($1<x<2$) on the surface under all conditions studied. The strong peak around 48 eV was assigned to the Mn 3p transition, while the weaker peak around 60 eV was due to the Co 3p transition. The peaks in the 63-65 eV window were tentatively attributed to Mn satellites in agreement with Oku and Hirokawa [42].

Surface fractions of Co probed by APXPS progressively decreased with both increasing reduction (200 mTorr H_2) temperature and reaction conditions. The 2p spectra of Co and Mn (shown in Figures 2b and 2c) were taken at photon energies of 900 and 760 eV, respectively, to give photoelectron energies of 120 eV. Co 2p core level spectra had very low and eventually no signal intensity after reduction in 200 mTorr H_2 at 350°C, as shown in Figure 1b. This absence of Co 2p/3p signal was believed to be the result of a densely packed MnO_x NP layer preventing the Co photoelectrons from reaching the analyzer.

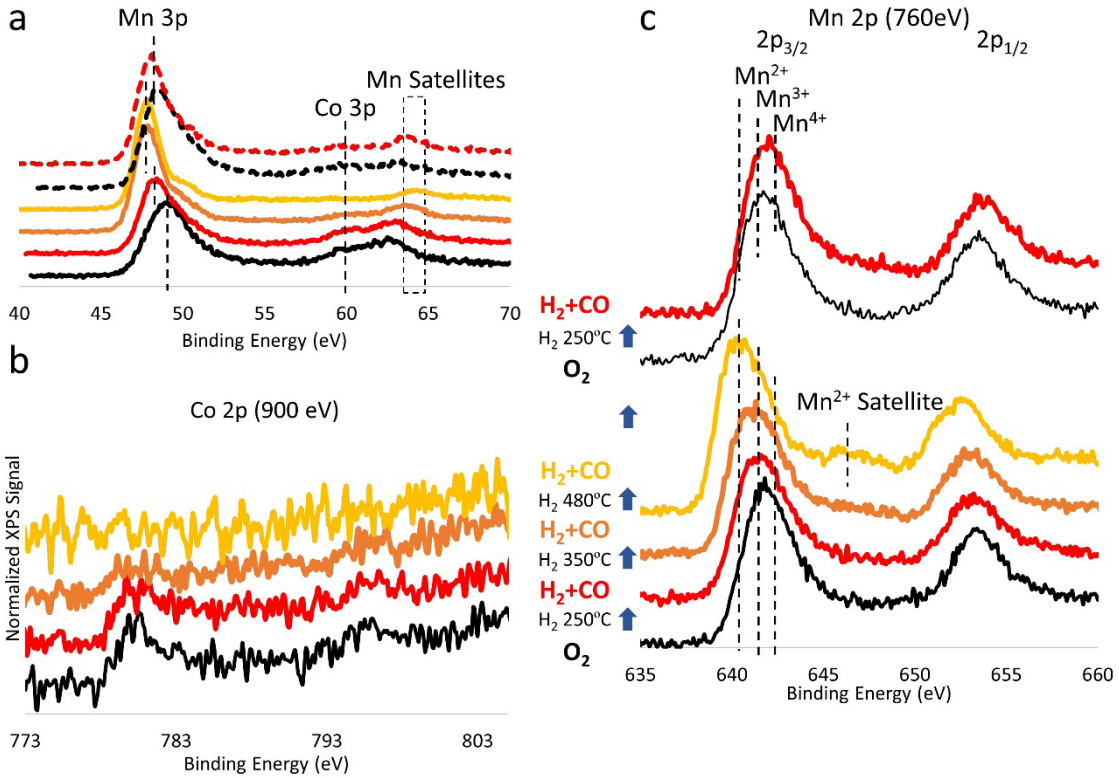

Fig. 1 Successive APXPS spectra showing (a) 3p core levels of Mn and Co, (b) 2p core levels of Co and (c) 2p core levels of Mn under various conditions. The spectra are stacked from bottom to top in the order of acquisition and color-coded as the key in the middle. APXPS spectra acquired in H_2 atmospheres (200 mTorr and 250, 350 and 480°C) are not plotted for clarity. Conditions are as described in the experimental section. In (a), Mn 3p and Co 3p levels are marked with dashed lines and Mn satellites with a dashed box. Dashed lines in (c) indicate the approximate peak positions for the respective oxidation states of Mn.

Mn 2p spectra indicated the progressive reduction of $MnO_{1<x<2}$ (1<x<2) NPs. Figure 1c shows shifts to lower binding energies with increasing reduction temperature and subsequent reaction conditions. Figure 1c also includes the Mn $2p_{3/2}$ peak assignments according to Nesbitt et. al [43]. The dominant oxidation state on the surface was identified as Mn^{3+} in H_2 atmospheres at 250°C and 350°C, and the following reactions at 225°C. In H_2 atmospheres at 480°C and the reaction conditions run afterward, MnO is the dominant surface species.

It should also be noted that MnO_x (1<x<2) NPs were reversibly oxidized in O_2 atmospheres at 350°C.

But Co not reversibly covered – it does not fully recover from H2 treatments…discuss this?

3.2.2 C and O 1s spectra

1s core level of C were monitored using 350, 630, 760 and 900 eV photons. O 1s was also probed using 630 eV photons

APXPS also indicated adsorption of CO on oxide surfaces. Clean C 1s XPS spectra were obtained in H_2 atmospheres following the oxidation in O_2 at 350°C. Under reaction conditions, two C 1s peaks were observed (Figure 2b); a peak at 291 eV from gas phase CO and a broader peak at 289 eV, which was attributed to CO adsorbed on MnO_x nanoparticles given their larger surface fractions. Furthermore, O 1s XPS spectra displayed an increase in surface CO at 531.5 eV and a decrease in lattice O at 530.5 eV under reaction conditions (Figure 2a). Combined C and O 1s normalized peak areas, as shown in Figure 2c, are indicative of CO adsorption on MnO_x (1<x<2) NPs, where a strong correlation exists for the increase of surface CO at the expense of lattice O.

Therefore, it was suggested that more CO was adsorbed for high manganese valences, while surface uptake of CO showed a minumum for MnO in Mn^{2+} state. +few more sentences

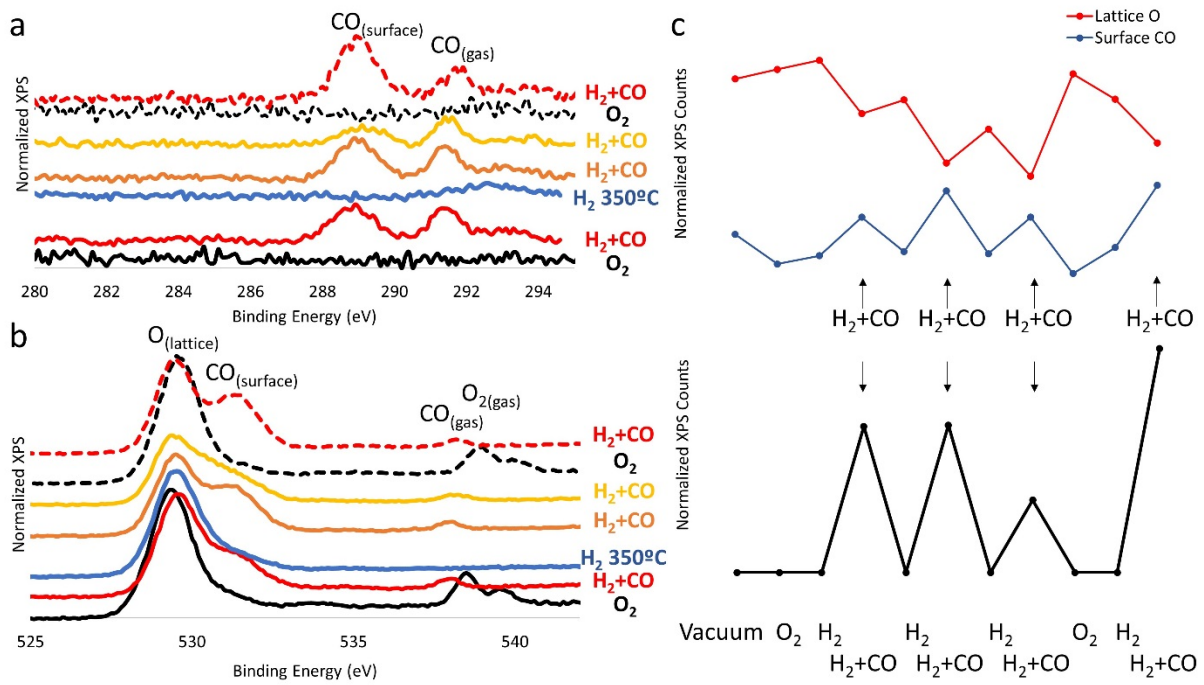

Fig 2. Successive APXPS spectra showing (a) C1s and (b) O1s core levels under various conditions. (c) Plots of normalized peak areas for lattice O and surface CO (from O1s [top] and C1s [bottom]). Spectra in (a) and (b) are stacked from bottom to top in the order of acquisition, and color-coded as in the middle key. APXPS spectra acquired in H_2 atmospheres, except H_2 at 350°C, are not plotted for clarity. Surface and gas phase CO are indicated in (a) and lattice O, surface CO, gas phase CO, and O_2 are indicated in (b). Arrows in (c) indicate successive reaction conditions following H_2 atmospheres at 250, 350 and 480°C from left to right.

3.3. *In Situ* Soft X-ray Absorption Spectroscopy (XAS)

3.3.1 Co and Mn L_3 edges

In situ XAS, probing the near surface regions of the MnO_x/Co_3O_4 catalyst, was used to quantitatively determine the oxidation states present on the surface through a linear combination fitting of reference compounds. Mn L_3 absorption edge spectra and the linear combination fittings are shown in Figure 3. Samples were run at both 7.8 (Figure 3a and b) and 32 (Figure 3c and 3d) Torr total reaction pressure after different reduction pre-treatments. The reduction temperature appears to have no significant effect on the oxidation state of MnO_x NPs during the CO hydrogenation reaction conditions, as shown in Figures 3a-c. The dominant oxidation states present measured after one hour under the reaction conditions are MnO and Mn_3O_4; however, prolonged reaction time in 32 Torr total reaction pressure produces MnO and MnO_2 at the expense of Mn_3O_4.

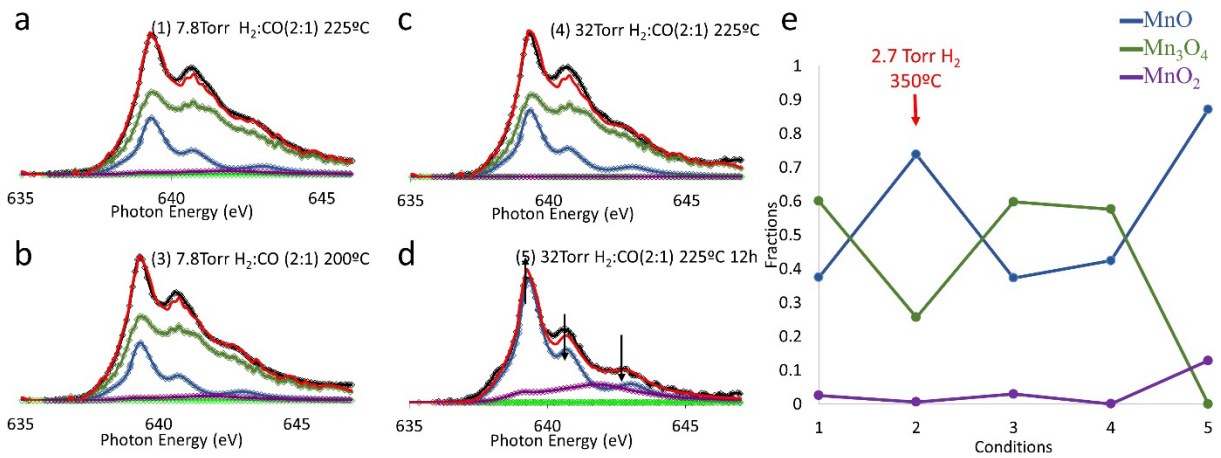

Fig. 3 (a-d) XAS TEY spectra at the Mn L_3 absorption edge during H_2+CO (2:1) reaction conditions. (e) Fractions of manganese species determined from the linear combination fittings in (a-d). XAS TEY spectrum in (a) was acquired following H_2 reduction at 250°C. XAS TEY spectra in (b-d) were acquired following H_2 reduction at 350°C. Spectra in (a-c) were acquired after the first hour under reaction conditions; (d) was acquired after 12 hours in the feed. The x-axis in (e) is numbered with the same codes as in the XAS TEY spectra; condition 2 is in H_2 atmosphere (TEY spectrum not shown) and is indicated with an arrow in (e). Arrows in (d) indicate the spectral changes relative to the previous spectrum.

The mesoporous oxide support was also found to actively change during reduction and reaction. Figure 4 displays the Co L_3 absorption edge and the resulting linear combination fits under various conditions. The dominant phase after reduction at 250°C and during reaction conditions of 7.8 Torr total pressure was spinel Co_3O_4 (Figure 4a). Following reduction at 350°C (Figure 4e, condition 2) Co_3O_4 was completely reduced to Co^{2+} species, namely CoO and $Co(OH)_2$, as shown in Figure 4 b-d. Upon increasing the total reaction pressure from 7.8 to 32 Torr, the relative amounts of $Co(OH)_2$ and CoO change by approximately 10%. However, unlike the MnO_x NPs, the Co does not undergo any further changes during prolonged reaction time (Figure 4d).

Coverage arguments? MnO has covered Co surface (from APXPS) such that it does not undergo further changes – it doesn't have surface exposed anymore

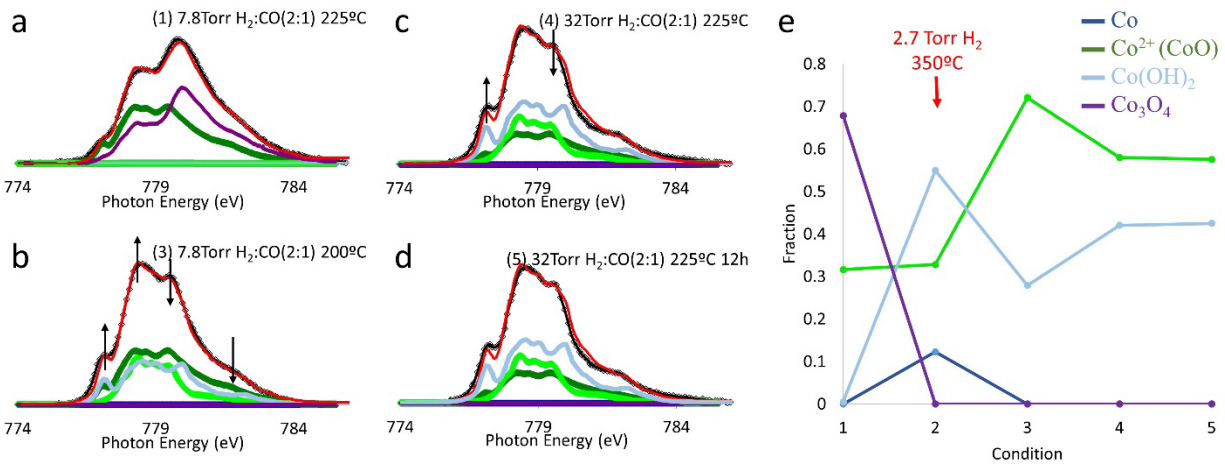

Fig. 4 (a-d) XAS TEY spectra at the Co L_3 absorption edge during H_2+CO(2:1) reaction conditions. Black connected diamonds are experimental spectra, red line is the fit, and the colored lines (e) Fractions of cobalt species determined from the linear combination fittings in (a-d). XAS TEY spectrum in (a) was acquired following H_2 reduction at 250°C. XAS TEY spectra in (b-d) were acquired following H_2 reduction at 350°C. Spectra in (a-c) were acquired after the first hour under reaction conditions; (d) was acquired after 12 hours in the feed. The x-axis in (e) is numbered with the same codes as in the XAS TEY spectra; condition 2 is in H_2 atmosphere (TEY spectrum not shown) and is indicated with an arrow in (e). XAS contributions for Co^{2+} in (e) was decomposed into two components in (a-d): Co^{2+} in octahedral sites, indicated with dark green; and Co^{2+} in tetrahedral sites, indicated with light green. Arrows in (b) and (c) indicate the spectral changes relative to the previous spectrum.

3.3.2 C and O K edges

C and O K absorption edge spectra are shown for various conditions in Figure 5. Pure O_2 spectra were taken while cooling from the oxidation treatment at 350°C, while pure CO and CO_2 spectra were taken at catalyst temperatures of 200°C for reference. The C K edge spectrum under H_2 shows the surface is free of residual carbon. Under 7.8 Torr reaction conditions, no apparent peak due to CO adsorption was observed; however, splitting and chemical shift of the gas phase CO peak (287.0 eV) were observed under 32 Torr reaction conditions, as shown in Figure 5a. In light of the APXPS findings, the splitting and shift of the gas phase CO peak could be due to adsorption of CO. Furthermore, gas phase CO_2 (290.4 eV) appears during reaction conditions. The gas phase CO_2 peak becomes more pronounced upon prolonged reaction periods, suggesting adsorption and reaction of CO on the oxide surfaces (MnOx surface?). The O K edge spectra support this view, with gas phase CO_2 (534.2 eV) appearing at long reaction times.

Discuss lattice O (~530 eV) decrease and CO2 increase

Discuss change in Mn valence to lower oxidation state/loss of lattice O

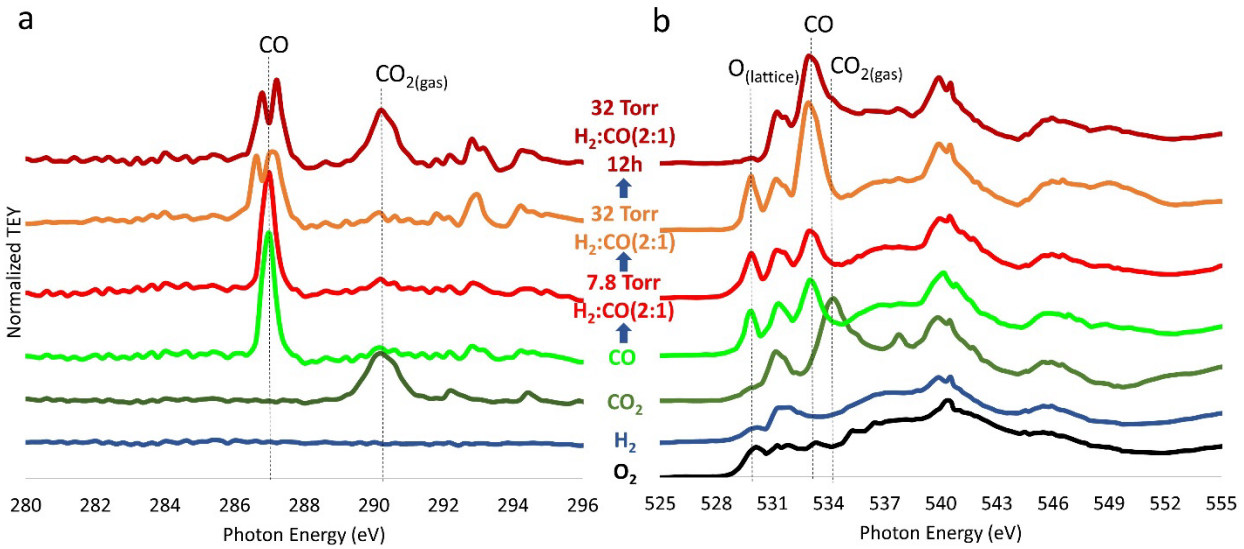

Fig. 5 XAS TEY spectra at the (a) C K and (b) O K absorption edges under various conditions. CO (gas phase and surface adsorbed) and gas phase CO_2 are indicated in (a) and (b). Lattice O is also indicated in (b). The O_2 spectrum was taken in vacuum after pumping out O_2 while cooling from 350°C. The H_2 spectra were taken in 2.7 Torr H_2 while cooling from 350°C. CO and CO_2 spectra were acquired in 2.7 Torr of the pure gases at 200°C. All H_2+CO(2:1) spectra were collected at 225°C. The spectra are shown in the order of acquisition from bottom to top.

3.3.3 Residual Gas Analysis

Using the quadruple mass spectrometer, we monitored various m/z species during the reaction of 32 Torr H_2+CO(2:1), after reduction at 350°C. Figure 6 shows the changes in the partial pressures of m/z 16 (CH_4), 18 (H_2O), 27 (hydrocarbon fragments), 28 (CO and hydrocarbon fragments) and 44 (CO_2) from 5 min to 11 hours into the reaction. A decrease in the m/z 28 signal was indicative of consumption of CO, as a corresponding increase in the partial pressure of CO_2 was observed. The observation of CO_2 is consistent with detection of gas phase CO_2 in the XAS TEY spectrum after 12 hours under reaction conditions. Interestingly, the formation of m/z 27 fragments and H_2O could be the result of the catalytic hydrogenation of CO, as water is a typical byproduct in C-C bond formation from CO hydrogenation. However, the formation of H_2O from a chemical reaction on the MnO_x surface cannot be ruled out. Also of note is the lack of CH_4 at the mass spectrometer; under low pressure CO hydrogenation conditions, CH_4 is often the most abundant product (ref?). In agreement with the mass spectroscopy data, no CH_4 is detected in the XAS TEY spectra. The qualitative agreement between the mass spec and XAS data is

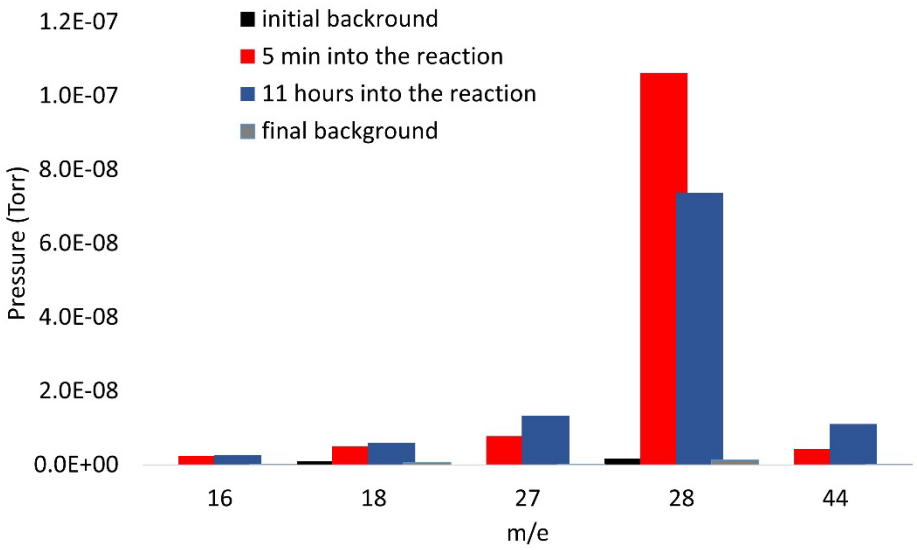

Fig 6. Partial pressures of various species before, during, and after the reaction of 32 Torr H_2+CO (2:1) at 225°C.

3.4. *Ex Situ* Spectro-microscopy

The catalyst was studied pre- and post-reaction using TEM, STEM/EDS and STXM. No changes to morphology in the post-reaction catalyst were detected by TEM or STEM. Elemental composition, measured by STEM/EDS remained uniform (Figure 7c-e). STEM/EELS spectra, acquired from single grains and multiple particles, indicated that the O/(Mn+Co) ratio dropped from 1.3 ± 0.1 for the fresh catalyst to 1.1 ± 0.2 for the spent catalyst, consistent with the reduction of catalyst. Representative energy loss spectra shown in Figure 8 clearly illustrate the loss of O content from the spent catalyst.

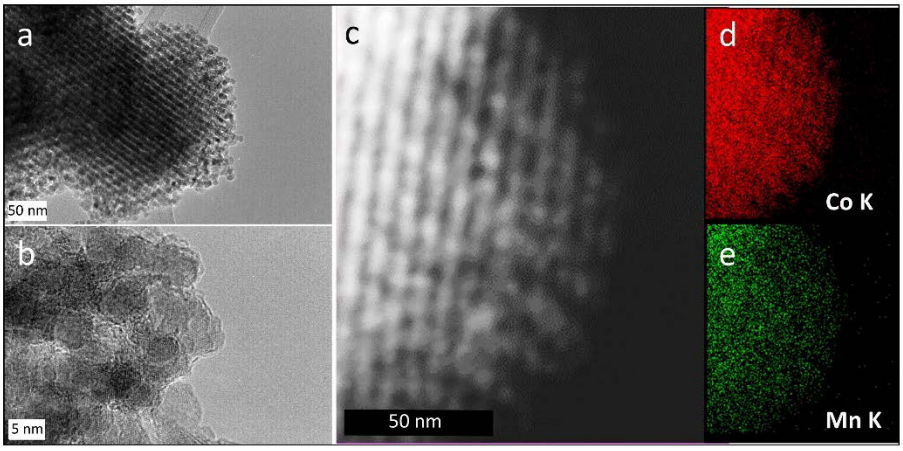

Fig 7. (a) TEM, (b) HRTEM and (c) STEM images of the post-reaction MnO_x NPs/m-Co_3O_4 catalyst. EDS elemental maps of the STEM image in (c) showing (d) Co K and (e) Mn K lines. Scale bars are given for each image.

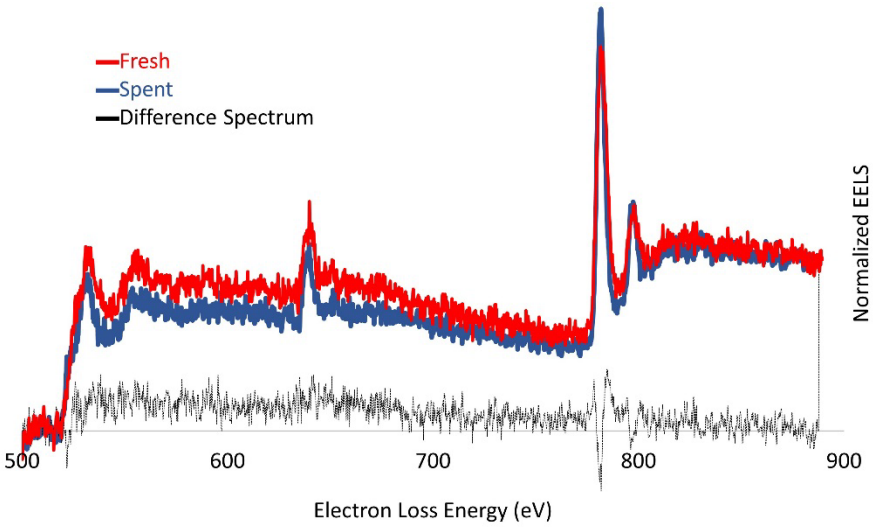

Fig 8. Representative STEM/EELS spectra of the pre- and post-reaction (i.e. fresh vs. spent) catalysts. Difference spectrum is also given.

STXM was performed on the pre- and post-reaction catalyst. Figure 9 shows the XAS spectra obtained by integrating over different sections of the STXM image, namely the core of the particle and the outer shell. The corresponding STXM maps are superimposed over the STXM image at the given photon energies. Changes from the pre-reaction to post-reaction catalyst are consistent with the XAS TEY spectra and the STEM/EELS O loss spectra discussed above; namely the Co L absorption edge shows a qualitative reduction from spinel Co_3O_4 in the pre-reaction catalyst (S2) to Co^{2+} species in the post-reaction catalyst (Figure 9b).

A visual inspection of the Mn L absorption edge XAS spectra revealed chemical shifts which were indicator of post-reaction oxidation of MnO NPs (see Figure 9a and Figure S2a). This could be a result of exposure to air, as in situ XAS found Mn^{2+} (major) and Mn^{4+} (minor) during reaction. This could also be a difference between surface and bulk of the catalyst particles, because in situ XAS TEY measured the near surface regions as opposed to the transmitted X-rays monitored by STXM. STXM also indicated that chemical compositions were uniform across single particles and over the entire catalyst, as shown by identical XAS spectra integrated over the core and shell of individual particles. Multiple particles were imaged and show consistent results.

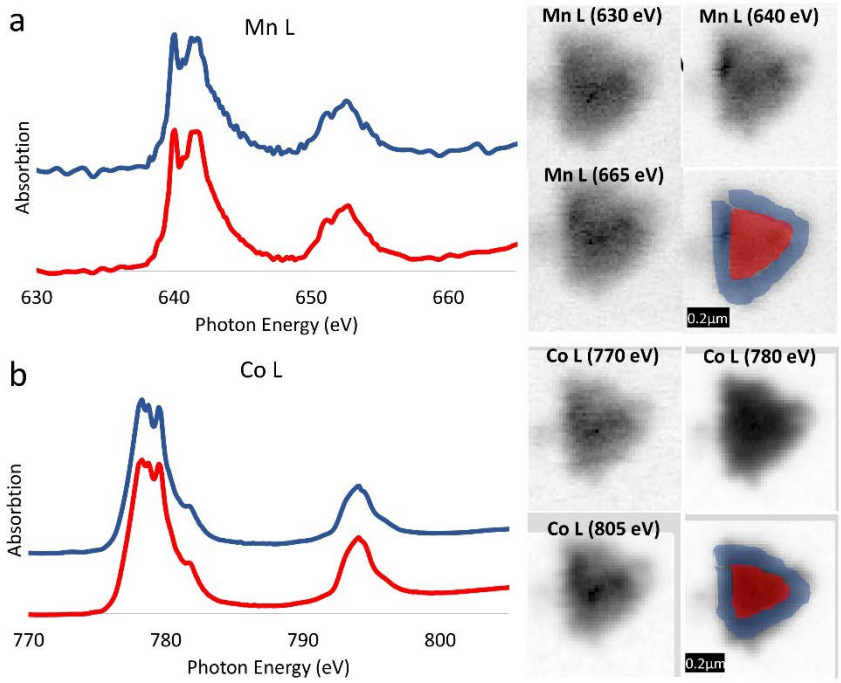

Fig 9. STXM spectra at (a) Mn L and (b) Co L absorption edges for the post-reaction catalyst. STXM spectra are color-coded as in the STXM images, and show integrated % absorption for the marked areas: particle cores (red) and particle shells (blue). STXM elemental maps are shown at given photon energies: 630 and 770 eV pre-edge; 640 and 780 eV, L_3 edge maxima; and 665 and 805 eV, post edge for Mn and Co, respectively.

4. Conclusion

In this paper, we studied the evolution of oxidation states and chemical compositions of a hybrid oxide catalyst comprised of MnO NPs supported on spinel Co_3O_4 with mesopores under H_2+CO atmospheres. Using tunable X-ray energies and reactive atmospheres of APXPS, we showed that MnO NPs covered cobalt oxide support; CO was adsorbed mainly on the MnO surfaces. *In situ* XAS TEY measurements revealed chemical compositions of MnO NPs and the oxide support at near surface regions and under H_2+CO reaction conditions: MnO and Mn_3O_4 were found dominant species for the nanoparticles, while hydroxide and oxides bearing +2 charge were obtained for the cobalt oxide support. *In situ* XAS TEY measurements also revealed CO_2 formation under 32 Torr H_2+CO (2:1) and at 225ºC after 12 hours of reaction, which also overlapped with the formation of MnO and MnO_2 at the expanse of Mn_3O_4 present early in the reaction. Combined APXPS, *in situ* XAS TEY and mass spectrometer measurements indicated the adsorption and reaction of CO over oxides of manganese and cobalt in the presence of H_2. Morphology and chemical composition of the catalyst were investigated using spectro-microscopy techniques, and found uniform across single particles and over particle ensembles.

References

[1] R.M. Rioux, B.B. Hsu, M.E. Grass, H. Song, G.A. Somorjai, Catal. Lett. 126 (2008) 10.
[2] Y. Yao, Z. Yan, L. Chen, Z. Zhou, L. Liu, D.W. Goodman, Catal. Lett. 142 (2012) 1437.
[3] V.V. Pushkarev, K. An, S. Alayoglu, S.K. Beaumont, G.A. Somorjai, J. Catal. 292 (2012) 64.
[4] Y.H. Niu, L.K. Yeung, R.M. Crooks, J. Am. Chem. Soc. 123 (2001) 6840.
[5] G.L. Bezemer, J.H. Bitter, H. Kuipers, H. Oosterbeek, J.E. Holewijn, X.D. Xu, F. Kapteijn, A.J. van Dillen, K.P. de Jong, J. Am. Chem. Soc. 128 (2006) 3956.
[6] T. Herranz, X. Deng, A. Cabot, J. Guo, M. Salmeron, J. Phys. Chem. B 113 (2009) 10721.
[7] V. Iablokov, S.K. Beaumont, S. Alayoglu, V.V. Pushkarev, C. Specht, J. Gao, A.P. Alivisatos, N. Kruse, G.A. Somorjai, Nano Lett. 12 (2012) 3091.
[8] A. Tuxen, S. Carenco, M. Chintapalli, C.-H. Chuang, C. Escudero, E. Pach, P. Jiang, F. Borondics, B. Beberwyck, A.P. Alivisatos, G. Thornton, W.-F. Pong, J. Guo, R. Perez, F. Besenbacher, M. Salmeron, J. Am. Chem. Soc. 135 (2013) 2273.
[9] S. Panigrahi, S. Basu, S. Praharaj, S. Pande, S. Jana, A. Pal, S.K. Ghosh, T. Pal, J. Phys. Chem. C 111 (2007) 4596.
[10] M.E. Grass, Y. Zhang, D.R. Butcher, J.Y. Park, Y. Li, H. Bluhm, K.M. Bratlie, T. Zhang, G.A. Somorjai, Angew. Chem.-Int. Ed. 47 (2008) 8893.
[11] M. Cargnello, V.V.T. Doan-Nguyen, T.R. Gordon, R.E. Diaz, E.A. Stach, R.J. Gorte, P. Fornasiero, C.B. Murray, Science 341 (2013) 771.
[12] M.A. El-Sayed, Acc. Chem. Res. 37 (2004) 326.
[13] G.A. Somorjai, S. Alayoglu, L.R. Baker, E. Gross, Abstr. Pap. Am. Chem. Soc. 244 (2012).
[14] R. Narayanan, M.A. El-Sayed, J. Phys. Chem. B 109 (2005) 12663.
[15] K.M. Bratlie, H. Lee, K. Komvopoulos, P. Yang, G.A. Somorjai, Nano Lett. 7 (2007) 3097.
[16] C.-K. Tsung, J.N. Kuhn, W. Huang, C. Aliaga, L.-I. Hung, G.A. Somorjai, P. Yang, J. Am. Chem. Soc. 131 (2009) 5816.
[17] S. Alayoglu, C. Aliaga, C. Sprung, G.A. Somorjai, Catal. Lett. 141 (2011) 914.
[18] V.V. Pushkarev, N. Musselwhite, K. An, S. Alayoglu, G.A. Somorjai, Nano Lett. 12 (2012) 5196.
[19] P. Christopher, S. Linic, Chemcatchem 2 (2010) 78.
[20] M. Crespo-Quesada, A. Yarulin, M. Jin, Y. Xia, L. Kiwi-Minsker, J. Am. Chem. Soc. 133 (2011) 12787.
[21] G.A. Somorjai, S.K. Beaumont, S. Alayoglu, Angew. Chem.-Int. Ed. 50 (2011) 10116.
[22] S. Alayoglu, F. Tao, V. Altoe, C. Specht, Z. Zhu, F. Aksoy, D.R. Butcher, R.J. Renzas, Z. Liu, G.A. Somorjai, Catal. Lett. 141 (2011) 633.
[23] J.R. Renzas, W. Huang, Y. Zhang, M.E. Grass, D.T. Hoang, S. Alayoglu, D.R. Butcher, F. Tao, Z. Liu, G.A. Somorjai, Phys. Chem. Chem. Phys. 13 (2011) 2556.
[24] G.A. Somorjai, Appl. Surf. Sci. 121 (1997) 1.
[25] K.M. Bratlie, K. Komvopoulos, G.A. Somorjai, J. Phys. Chem. C 112 (2008) 11865.
[26] C.J. Kliewer, C. Aliaga, M. Bieri, W. Huang, C.-K. Tsung, J.B. Wood, K. Komvopoulos, G.A. Somorjai, J. Am. Chem. Soc. 132 (2010) 13088.
[27] C. Aliaga, C.-K. Tsung, S. Alayoglu, K. Komvopoulos, P. Yang, G.A. Somorjai, J. Phys. Chem. C 115 (2011) 8104.
[28] D.F. Ogletree, H. Bluhm, G. Lebedev, C.S. Fadley, Z. Hussain, M. Salmeron, Rev. Sci. Instrum. 73 (2002) 3872.

[29] F. Tao, M.E. Grass, Y. Zhang, D.R. Butcher, J.R. Renzas, Z. Liu, J.Y. Chung, B.S. Mun, M. Salmeron, G.A. Somorjai, Science 322 (2008) 932.
[30] F. Tao, M.E. Grass, Y. Zhang, D.R. Butcher, F. Aksoy, S. Aloni, V. Altoe, S. Alayoglu, J.R. Renzas, C.-K. Tsung, Z. Zhu, Z. Liu, M. Salmeron, G.A. Somorjai, J. Am. Chem. Soc. 132 (2010) 8697.
[31] K. An, S. Alayoglu, N. Musselwhite, S. Plamthottam, G. Melaet, A.E. Lindeman, G.A. Somorjai, J. Am. Chem. Soc. 135 (2013) 16689.
[32] K. Na, N. Musselwhite, X. Cai, S. Alayoglu, G.A. Somorjai, J. Phys. Chem. A (2014).
[33] G. Melaet, W.T. Ralston, C.-S. Li, S. Alayoglu, K. An, N. Musselwhite, B. Kalkan, G.A. Somorjai, J. Am. Chem. Soc. 136 (2014) 2260.
[34] C.-S. Li, G. Melaet, W.T. Ralston, K. An, C. Brooks, Y. Ye, Y.-S. Liu, J. Zhu, J. Guo, S. Alayoglu, G.A. Somorjai, Nat. Commun. 6 (2015) 6538.
[35] G.L. Bezemer, U. Falke, A.J. van Dillen, K.P. de Jong, Chem. Commun. (2005) 731.
[36] F. Morales, F.M.F. de Groot, P. Glatzel, E. Kleimenov, H. Bluhm, M. Hävecker, A. Knop-Gericke, B.M. Weckhuysen, J. Phys. Chem. B 108 (2004) 16201.
[37] S. Werner, G.R. Johnson, A.T. Bell, ChemCatChem 6 (2014) 2881.
[38] J. Park, K.J. An, Y.S. Hwang, J.G. Park, H.J. Noh, J.Y. Kim, J.H. Park, N.M. Hwang, T. Hyeon, Nat. Mater. 3 (2004) 891.
[39] Y. Ren, Z. Ma, L. Qian, S. Dai, H. He, P.G. Bruce, Catal. Lett. 131 (2009) 146.
[40] M.E. Grass, P.G. Karlsson, F. Aksoy, M. Lundqvist, B. Wannberg, B.S. Mun, Z. Hussain, Z. Liu, Rev. Sci. Instrum. 81 (2010) 053106.
[41] T. Warwick, H. Ade, D. Kilcoyne, M. Kritscher, T. Tylisczcak, S. Fakra, A. Hitchcock, P. Hitchcock, H. Padmore, J. Synchrotron Radiat. 9 (2002) 254.
[42] M. Oku, K. Hirokawa, S. Ikeda, J. Electron Spectrosc. Relat. Phenom. 7 (1975) 465.
[43] H.W. Nesbitt, D. Banerjee, Am. Mineral. 83 (1998) 305.

Acknowledgements